# QEXAFS Investigation of the Particle Growth of PtRh Clusters Supported on NaY

**F. Cimini and R. Prins***

*Laboratory of Technical Chemistry, Swiss Federal Institute of Technology (ETH), Universitätstrasse 6, 8092 Zürich, Switzerland*

*Received: December 11, 1996; In Final Form: March 26, 1997*[⊗]

The quick EXAFS technique was used to study the formation and growth of bimetallic PtRh particles in zeolite NaY during reduction. Before reduction, only metal−oxygen signals were detectable. While increasing the temperature at a rate of 5 °C/min and passing $H_2$ through the in situ cell, 1 min EXAFS scans were recorded at the Rh and Pt edges. At 40 °C, an intense Rh−Rh signal suddenly appeared, indicating the formation of small monometallic Rh clusters. The remaining Rh−O signal slowly decreased between 100 and 200 °C, simultaneous with the appearance and slow growth of a small Rh−Pt signal. The Pt edge EXAFS changed less abruptly than the Rh edge EXAFS. Above 80 °C, the Pt−O signal started to decrease, and at 100 °C Pt−Pt and Pt−Rh signals appeared simultaneously, pointing to the formation of small bimetallic particles. These signals grew slowly until 300 °C, even after the Pt−O signal had disappeared. This indicates that small bimetallic particles move through the channels of the zeolite and merge to form larger particles. This merging should also involve the big monometallic Rh clusters formed at 40 °C, probably situated in the supercages of the zeolite. At the end of the reduction, two kinds of clusters were present: one having a Rh core, possibly also completely monometallic, the other consisting of Pt-rich bimetallic PtRh clusters. The different reduction behavior of Rh and Pt leads to a nonhomogeneous composition of the metal particles, although they all have a similar size.

## Introduction

Extended X-ray absorption fine structure (EXAFS) has been found to be valuable probe for establishing the presence of bimetallic clusters and for obtaining information on their structure.[1−7] In our previous article we made use of the EXAFS technique to prove that bimetallic Rh−Pt particles were obtained in NaY zeolite.[8] On the other hand, the information provided by the EXAFS technique (i.e., number and kind of neighboring atoms and interatomic distances) are *average* data and are difficult to interpret in the case of nonhomogeneity of the clusters.[9] To overcome this problem, we investigated the reduction of our bimetallic Rh−Pt/NaY sample with the quick EXAFS (QEXAFS) technique as well.

In a conventional EXAFS measurement the photon energy is scanned in a step-by-step mode, yielding a spectrum of very high accuracy in 30−50 min. The QEXAFS technique allows an EXAFS spectrum to be recorded in a much shorter period of time (50−100 s), but with a loss of data quality and energy range. The scan time is reduced by moving the monochromator at a constant angular speed and recording the data "on the fly", eliminating the overhead time associated with moving the monochromator on a point-by-point basis.[10] It is, therefore, possible to use this technique to investigate processes that change with time.

Studies have already been dedicated to the formation and growth of metallic particles supported on NaY zeolite, and conventional EXAFS measurements were also carried out at different stages of preparation (drying, calcination, reduction).[11−14] An analysis that allows the direct investigation of the evolution of the metal atoms into metal clusters has not yet been made. The aim of the present work is to understand the fate of the Rh and Pt atoms during the genesis of the metal atoms and their growth to bimetallic Rh−Pt clusters on zeolite NaY. A series of QEXAFS spectra was, therefore, recorded at each absorption edge (Pt $L_{III}$ and Rh K) during reduction, and each single spectrum was subsequently analyzed. For comparison, the reduction of a monometallic Pt sample was also studied. An understanding of the reduction mechanism should offer interesting possibilities for the future design of clusters. Similar, but not exactly the same information can be obtained by performing a series of traditional EXAFS analyses after reducing the sample to successively higher reduction temperatures, followed by quenching to low temperature for the EXAFS measurement.

## Experimental Section

The QEXAFS spectra were measured at the Synchrotron Radiation Source (SRS) in Daresbury (UK) running at 2 GeV with an electron current ranging from 180 to 220 mA. The data were recorded at station 9.2 (transmission setup) which receives the X-ray radiation from a 5 T multipole superconducting wiggler. A bent Si 220 double-crystal monochromator was used, with the second crystal detuned to 50% of the maximum intensity for higher harmonic rejection. Ionization chambers filled with a mixture of Ar and He were employed as detectors, and the Ar/He mixture was chosen to give 20% absorption in the chamber before the measuring cell and 80% in the chamber after the cell.

The bimetallic sample was prepared by the ion-exchange method, adding zeolite NaY (Chemie Uetikon) to an aqueous solution of $Pt(NH_3)_4(NO_3)_2$ (Johnson Matthey) and $Rh(NO_3)_3 \cdot 2H_2O$ (Johnson Matthey) and stirring the mixture for 24 h. The mixture was filtered and washed, and the recovered solid was dried at 100 °C and calcined at 300 °C for 2 h under oxygen flow. The final metal contents, measured by atomic absorption spectroscopy, were 2.6 wt % Pt and 1.3 wt % Rh, corresponding approximately to a molar ratio 1:1. This sample will be referred to as A. A 5.0 wt % Pt monometallic sample (B) was prepared in a similar way.

To obtain a self-supporting wafer with an absorbance of about 2.5 for the QEXAFS measurements at the Pt as well as at the

[⊗] Abstract published in *Advance ACS Abstracts,* June 15, 1997.

S1089-5647(96)04052-7 CCC: $14.00 

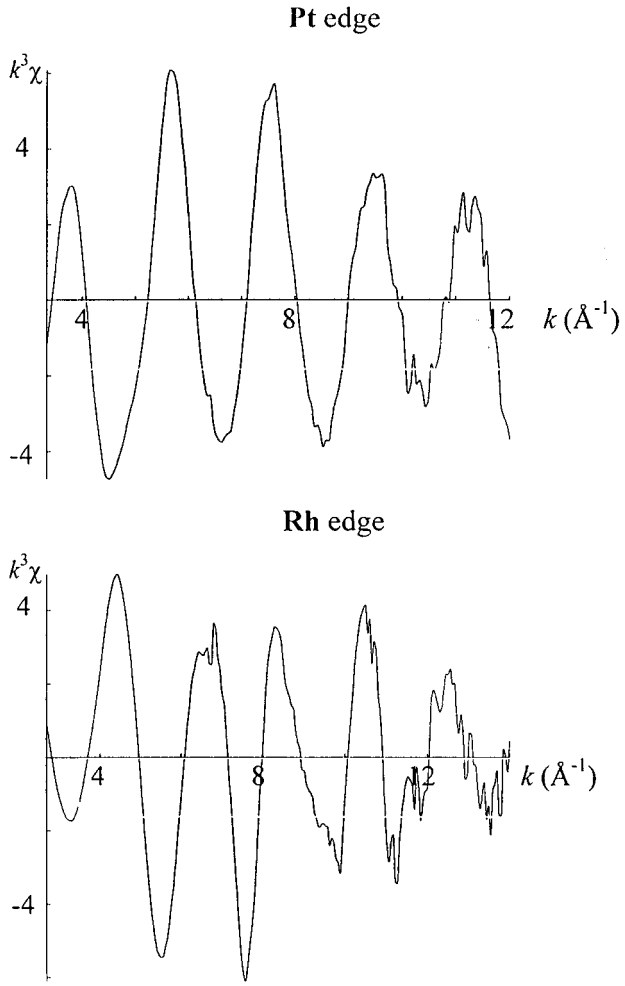


**Figure 1.** $\chi(k)k^3$ spectra of sample A before reduction, measured at the Pt (above) and Rh (below) absorption edges.

Rh absorption edge, two samples had to be prepared by pressing the right amount of sample into a sample holder. The sample holder was mounted in an in situ transmission cell[15] and transferred into the working hutch. To find the best compromise among the energy range of the spectrum, the scanning speed, and the signal-to-noise ratio, some test spectra were recorded at each absorption edge. The following operating conditions were chosen: a 1 min scan from −30 to 570 eV relative to the energy threshold at the Pt edge and a 1 min scan from −30 to 750 eV at the Rh edge. Figure 1 shows the $k^3\chi$ spectra of sample A obtained under these conditions.

The reduction was started by increasing the temperature of the cell with the heater and by simultaneously passing $H_2$ through the cell. The cell temperature was raised to 300 °C with a heating rate of 5 °C/min and kept for 2 h at 300 °C. During the measurement of a single scan, temperature increases, and the sample may react further with hydrogen. The spectrum is, therefore, an asymmetric *average* of the situation over the recording minute, the low-energy part being recorded at a slightly lower temperature as the high-energy side. In all cases but one (see below), this was acceptable because of the relatively low speed of reduction.

During reduction, which took about 3 h, QEXAFS spectra were continuously recorded, yielding 180 spectra in all. This procedure was carried out at the Pt $L_{III}$ absorption edge of one sample A, at the Rh K absorption edge of another A sample (with the right absorbance) and at the Pt $L_{III}$ absorption edge of sample B. All spectra, with the exception of a few that had a low S/N ratio, were analyzed qualitatively, and the most significant ones were studied also quantitatively.

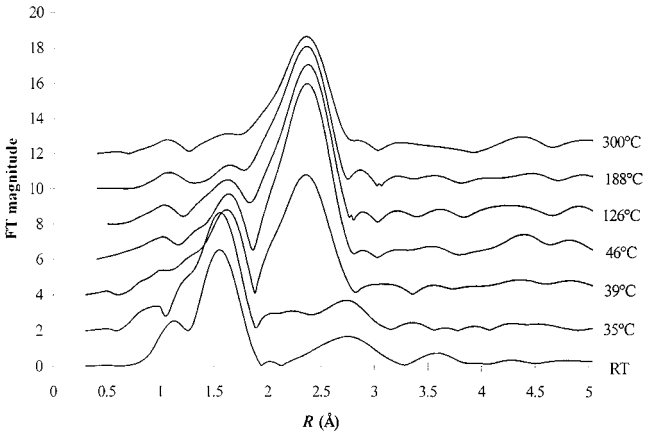


**Figure 2.** Evolution of the FT of $\chi(k)k^3$ measured at the Rh edge during reduction of sample A.

The standard data reduction procedure was employed to isolate the EXAFS oscillation from the raw spectra.[16,17] This consists of deglitching, preedge subtraction, background subtraction, normalization, and Fourier transformation. The quantitative analyses were performed by means of a fitting procedure after isolating the shell(s) of interest by an inverse Fourier transformation. The backscattering amplitudes and phase shifts of the Rh−Rh and Pt−Pt contributions were obtained from the EXAFS signals of the pure metal foils, measured at the same temperature as the spectrum under analysis, to limit the anharmonicity problems caused by the high temperature. To do so, it was necessary to measure the EXAFS signals of the Rh and Pt foils at many different temperatures between room temperature and 300 °C. As for the **Pt**−Rh (Pt is the absorber) and **Rh**−Pt contributions, we used phase shift functions obtained from FEFF codes[18] and experimental backscattering amplitude functions extracted from Pt foil, when Pt was the backscatterer atom (**Rh**−Pt), and from Rh foil when Rh was the backscatterer (**Pt**−Rh). The transferability of the backscattering amplitude from a pure metal foil to a system with a different absorber atom but the same backscatterer has been used before with satisfactory results.[19−21] As shown in the preceding paper,[8] the analysis of EXAFS spectra of PtRh foils confirmed the reliability of the transferability of the backscattering amplitudes. The coordination numbers and interatomic distances were determined by multiple-shell fitting in $k$ space and in $R$ space, using $k^1$ as well as $k^3$ weighting.

Although our method of measuring reference spectra at all temperatures decreased the anharmonicity problems caused by the high temperature, the question remains if the parameters extracted from the reference metal foils are applicable to the small metal clusters. Small metal clusters have lower Debye temperatures as bulk metals, and this will influence the quantitative results. Therefore, although the trends and qualitative conclusions remain unaltered, the obtained results should be viewed as semiquantitative rather than quantitative.

## Results

Two kinds of information were extracted from the data. Qualitative information was provided by the Fourier transform (FT) profiles of the EXAFS data, which visualize the evolution of the metal environment during the reaction. Quantitative results were obtained by the full EXAFS analysis, performed on the most significant spectra recorded.

**Rh Edge.** We start by considering sample A, measured at the Rh edge. The evolution of the FT of the $k^3$-weighted

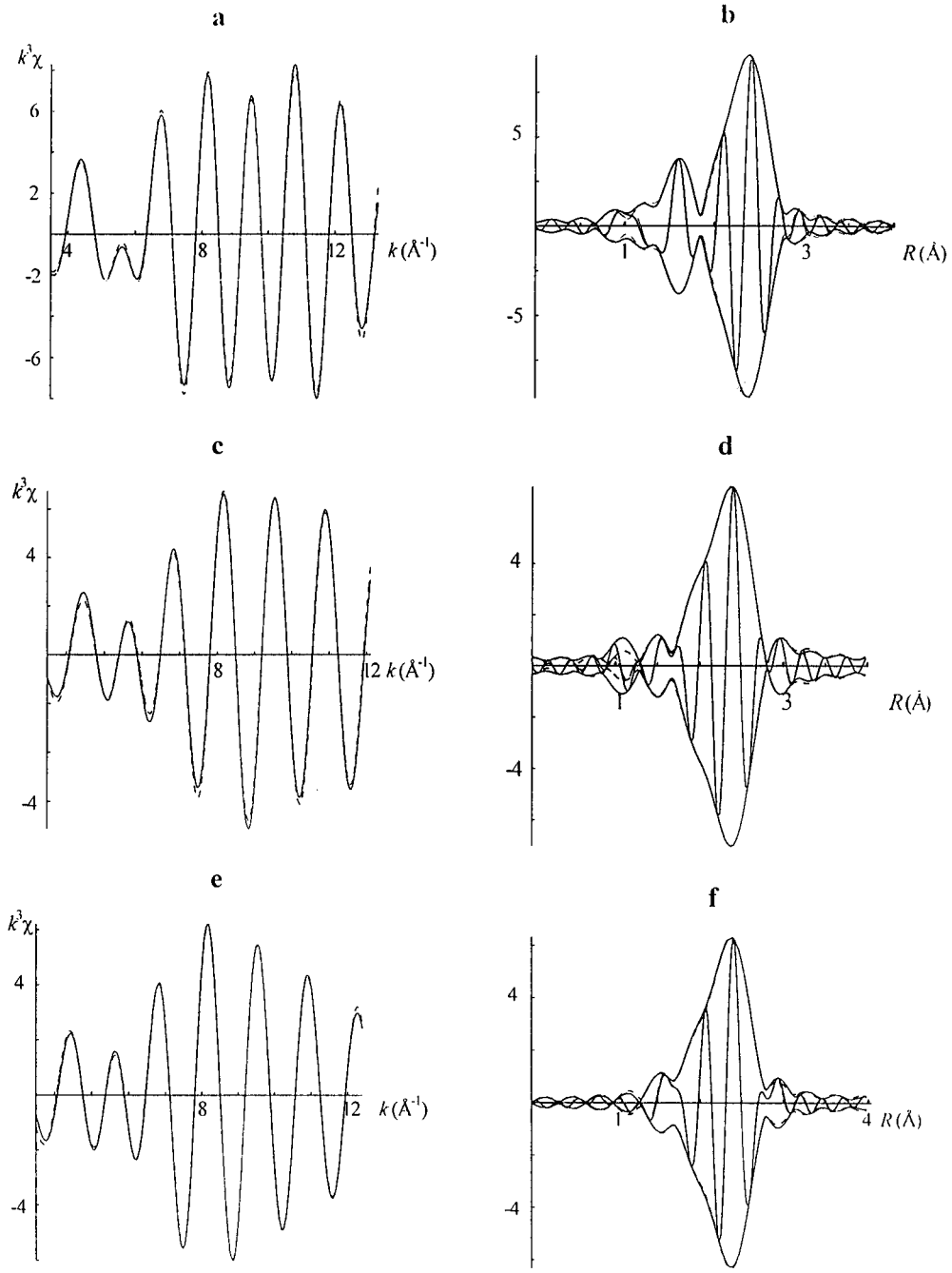


**Figure 3.** Sample A during reduction (Rh edge): measured signals (—) and corresponding fits (− − −) of $\chi(k)k^3$ and related FT at 46 °C (**a** and **b**, respectively), 188 °C (**c** and **d**, respectively), and 254 °C (**e** and **f**, respectively).

EXAFS is represented in Figure 2. Before reduction (room temperature, RT), two peaks are visible. The first peak at 1.5 Å represents a **Rh**−O signal, probably due to Rh oxides formed in the zeolite after the calcination at 300 °C. The second peak at 2.7 Å can be attributed to a **Rh**−Rh signal belonging to $Rh_2O_3$, which has a Rh−Rh interatomic distance of 3.01 Å, expected to peak around 2.7−2.9 Å because of the phase shift of the interatomic distances in the FT.[22] Between RT and 35 °C only small differences are found around 2.5 Å. At 39 °C a large peak at 2.3 Å suddenly appeared, simultaneous with the disappearance of the **Rh**−Rh signal (from $Rh_2O_3$) and with a decrease in the **Rh**−O signal. The peak at 2.3 Å, corresponding to a real distance of about 2.7 Å from the absorber (Rh), indicates the presence of Rh metal particles. After a further increase in the metal−metal peak at 46 °C, the FT profile did not change significantly until 104 °C. From 104 to 188 °C the Rh−O signal decreased slowly, while the Rh−Rh peak hardly changed. After the disappearance of the **Rh**−O signal at about 180 °C, the FT profile remained almost unchanged until the end of the reduction. Only a small contraction of the metal−metal peak could be detected, probably related to the increase in the temperature and consequently in the Debye−Waller factor ($\sigma^2$).

Some of the recorded EXAFS spectra were analyzed quantitatively to obtain detailed information about the coordination numbers (CN) and interatomic distances. After isolation of the first shell region (1−3 Å) by an inverse Fourier transformation, a typical *k*-space (wave vector space) range for the fitting procedure was 3−12.5 Å$^{-1}$. Considering the *k*- and *R*-space ranges, it was thus possible to reliably fit three different shells.[23] Some fits are depicted in Figure 3. Figure 4a represents the evolution of the coordination numbers at the Rh edge during reduction. Table 1 lists the complete results of quantitative analyses. They confirm the conclusions reached in the qualita-

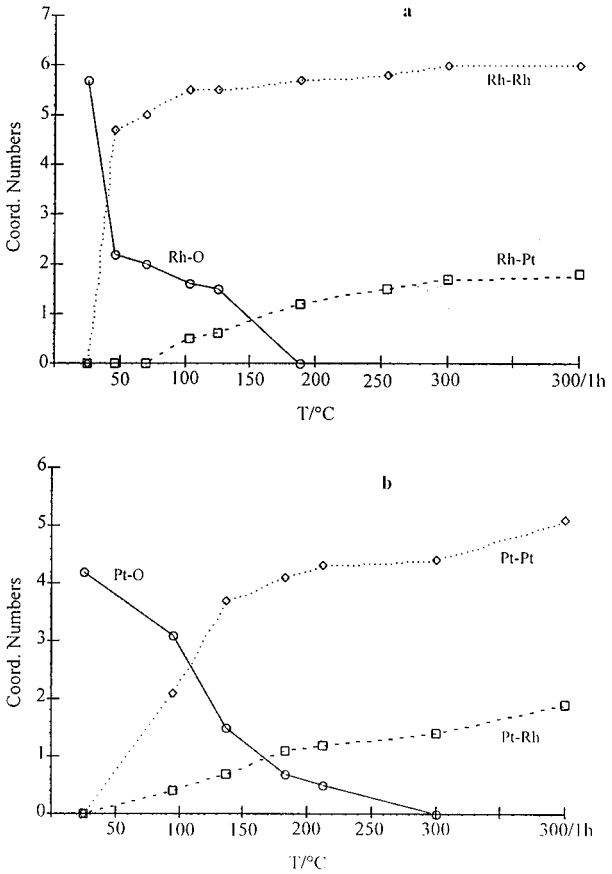


**Figure 4.** Evolution of the coordination numbers at the Rh (**a**) and Pt (**b**) edges during reduction of sample A.

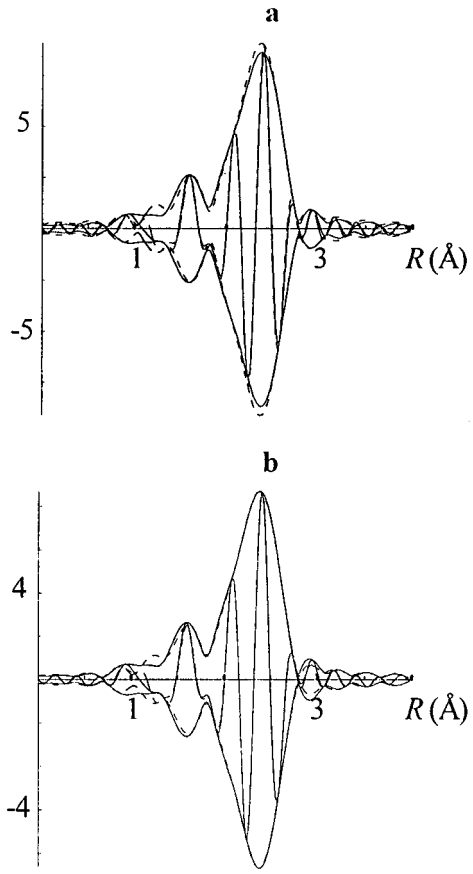


**Figure 5.** Sample A during reduction at 104 °C (Rh edge). FT of $\chi(k)k^3$ (—) and related fit (– – –) without (**a**) the **Rh**−Pt contribution (variance of fit = 0.0156) and with (**b**) the **Rh**−Pt contribution (variance of fit = 0.0048).

**TABLE 1: Structural Parameters of Sample A at the Rh Edge during Reduction (Fits: $\Delta k = 3-12.5$ Å$^{-1}$, $\Delta R = 1-3$ Å, Variance ≈ 0.004)**

| absorb | backsc | *CN* | *R* (Å) | $\Delta\sigma^2$ | *T* (°C) |
|---|---|---|---|---|---|
| Rh | O | 5.7 | 2.02 | 0.0011 | RT |
| Rh | Rh | 1.8 | 3.01 | 0.0052 | |
| Rh | O | 2.2 | 2.03 | 0.0013 | 46 |
| Rh | Rh | 4.7 | 2.69 | 0.0024 | |
| Rh | O | 2.0 | 2.03 | 0.0015 | 70 |
| Rh | Rh | 5.0 | 2.69 | 0.0026 | |
| Rh | O | 1.6 | 2.04 | 0.0012 | 104 |
| Rh | Rh | 5.5 | 2.69 | 0.0010 | |
| Rh | Pt | 0.5 | 2.71 | 0.0032 | |
| Rh | O | 1.5 | 2.04 | 0.0011 | 126 |
| Rh | Rh | 5.5 | 2.67 | 0.0008 | |
| Rh | Pt | 0.6 | 2.72 | 0.0031 | |
| Rh | Rh | 5.7 | 2.69 | 0.0016 | 188 |
| Rh | Pt | 1.2 | 2.73 | 0.0004 | |
| Rh | Rh | 5.8 | 2.69 | 0.0011 | 254 |
| Rh | Pt | 1.5 | 2.73 | 0.0002 | |
| Rh | Rh | 6.0 | 2.68 | 0.0013 | 300 |
| Rh | Pt | 1.7 | 2.74 | 0.0002 | |
| Rh | Rh | 6.0 | 2.68 | 0.0010 | 300/1 h |
| Rh | Pt | 1.8 | 2.73 | 0.0004 | |

tive analysis and enabled an accurate determination of the dimensions of the particles involved in the reduction. $Rh_2O_3$ particles are present after calcination and before reduction, as shown by the interatomic distances, which were almost identical with those of $Rh_2O_3$. Comparison of the Rh−Rh coordination number (CN) of 1.8 with that of bulk $Rh_2O_3$, CN = 3, indicates that the size of the $Rh_2O_3$ particles is quite small and are most likely situated in the supercages of the NaY zeolite. The presence of rhodyl ions $(RhO)^+$ as well as $Rh^+$ or $Rh^{3+}$ ions, which proved to be present in similar cases,[24,25] cannot be excluded, but evidence to support this hypothesis was not found. The identification of Rh ions bonded to the oxygen atoms of the zeolite framework would in any case be difficult, because a Rh−O contribution around 2 Å would be indistinguishable from that due to $Rh_2O_3$. Temperature-programmed reduction (TPR) spectra of monometallic Rh samples prepared analogously indicated an average oxidation state of 3.2. The determination of the oxidation state from the TPR of the bimetallic sample would be quite uncertain, because it is dependent on the oxidation state of the second metal atom. The presence of $Rh^{IV}$ is, therefore, conceivable. However, the Rh−O distance expected for $RhO_2$, 1.93 Å, was not detected.

It was impossible to obtain an acceptable fit of the spectrum recorded at 39 °C. This must be due to the evolution of the sample during the scan. In this case (the only one among all the recorded spectra), the evolution was very quick, and the signal recorded at the end of the scan is due to particles which are different from those that produced the signal at the beginning of the scan. A large Rh−Rh contribution was detected at 46 °C. The Rh−Rh interatomic distance (2.69 Å) is very similar to that of pure metal (2.68 Å), indicating the presence of Rh metal clusters. To obtain the real coordination number of the Rh atoms in the metal clusters, the observed coordination number of 4.7 was normalized for the presence of rhodium oxide. The resulting coordination number of 6.5 indicates that small clusters were formed. At the same time, the Rh−O CN decreased remarkably, suggesting that about one-third to one-quarter of the Rh atoms is still present in the oxidic form.

The situation did not change significantly until 104 °C, when a small **Rh**−Pt (CN = 0.5) signal appeared. This contribution did not substantially modify the FT profile, but its presence clearly improved the fitting quality, as shown in Figure 5. The

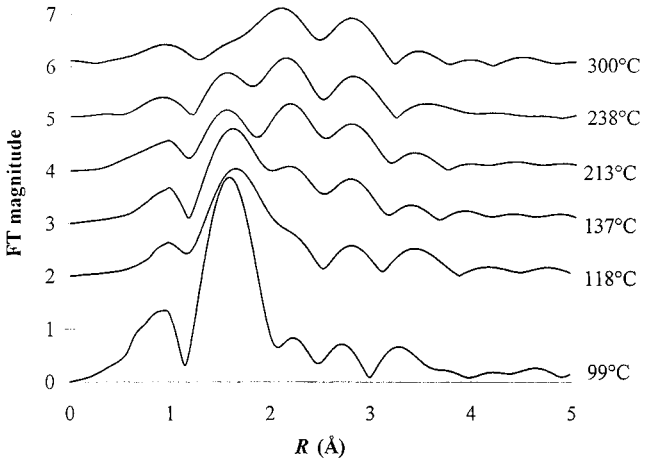


**Figure 6.** Evolution of the FT of $\chi(k)k^3$ measured at the Pt edge during reduction of sample A.

interatomic distance of 2.71 Å is in good agreement with what is expected of such a metal−metal bond.

The subsequent spectra (not all reported in Table 1) pointed to a gradual growth of the **Rh**−Pt signal, simultaneous with a decrease in the Rh−O signal. At 188 °C, the Rh−O contribution had disappeared, and the **Rh**−Pt CN was equal to 1.2. From 188 to 300 °C only a very small increase in the two metal−metal (**Rh**−Rh and **Rh**−Pt) contributions occurred. At the end of the reduction, the **Rh**−Rh CN was 6 and the **Rh**−Pt CN 1.8. The $\chi$ spectrum also continued to change slightly during the isothermal reduction at 300 °C, thus causing a small change in the CNs and interatomic distances. No relevant differences were detected in the spectra recorded after more than 1 h at 300 °C.

**Pt Edge.** The FT of the $k^3$-weighted EXAFS spectra of sample A, measured at the Pt edge, are represented in Figure 6. Before the reduction (not shown) a large peak was present at 1.6 Å, which is due to a Pt−O signal from Pt oxides and/or $Pt^{2+}$ bonded to the oxygen atoms of the zeolite framework. From RT to 99 °C a contraction of the Pt−O signal took place with no evidence of new peaks; however, in the region 2−3 Å, a qualitative distinction between side lobes and real peaks is very problematic. At 118 °C a shoulder to the right of the Pt−O signal, around 2.2 Å, appeared, and at 137 °C this shoulder had grown in size and an additional small peak appeared at 2.8 Å. From 118 to 253 °C a gradual decrease in the Pt−O signal, together with a gradual increase in the signals at 2.2 and 2.8 Å, were observed. The latter signals are attributed to the two overlapping metal−metal coordination shells (**Pt**−Pt and **Pt**−Rh). After the disappearance of the Pt−O signals, the two metal−metal signals continued to change slightly. Two opposing effects may play a role: on one hand the growth of the particles will cause an enlargement of the peaks, and on the other hand the increase in the temperature, and consequently in the Debye−Waller factor, will effect a decrease. The FT of the spectra recorded at the end of the temperature ramp were considerably different from that recorded after 1 h at 300 °C.

In the case of Pt, the quantitative analysis confirmed the qualitative conclusions and revealed new information. Some of the results are reported in Table 2, and some of the fits are shown in Figure 7. Figure 4b shows the evolution of the coordination numbers at the Pt edge during reduction. The typical *R* range for the inverse Fourier transformation was 1−3 Å and the *k* range for the fitting procedure was 3.5−12 $Å^{-1}$. Before reduction, two different Pt−O signals were present: 0.9 O at 1.95 Å and 3.3 O at 2.04 Å, ascribed to different Pt oxides species, i.e., PtO and $PtO_2$. In the latter compound each Pt atom has 4 O neighboring atoms at 1.976 Å.[26] The TPR spectra of monometallic Pt samples prepared in a similar way indicated that 2.7 is the average oxidation number, thus suggesting that a considerable number of the Pt atoms is present as $Pt^{IV}$. Park et al. obtained a similar result for Pt supported on HY.[27] Unfortunately, a precise assignment of the EXAFS signals is problematic because of the probable, contemporary presence of $Pt^{2+}$ ions bonded directly to the oxygen atoms of the zeolite framework at interatomic distances which are not exactly defined. In a similar case, Tzou et al.[12] found that the Pt atoms were mostly present as $Pt^{2+}$ ions. In addition, the second small peak at 3.5 Å could not be identified. It is probably due to the overlap of second coordination shell contributions from various Pt atoms, for instance Pt−O of Pt oxides, and Pt−O and Pt−Si of Pt ions bonded to the framework. However, the small size of the second peak, together with the Pt−O coordination numbers, points to the presence of very small Pt oxide particles (PtO, $PtO_2$) and isolated Pt ions.

**TABLE 2: Structural Parameters of Sample A at the Pt Edge during Reduction (Fits: $\Delta k = 3-11.5$ $Å^{-1}$, $\Delta R = 1-3$ Å, Variance ≈ 0.004)**

| absorb | backsc | *CN* | *R* (Å) | $\Delta\sigma^2$ | *T* (°C) |
|---|---|---|---|---|---|
| Pt | O | 0.9 | 1.95 | 0.0017 | RT |
| Pt | O | 3.3 | 2.04 | 0.0010 | |
| Pt | O | 3.1 | 2.02 | 0.0018 | 95 |
| Pt | Pt | 2.1 | 2.70 | 0.0013 | |
| Pt | Rh | 0.4 | 2.68 | 0.0034 | |
| Pt | O | 1.5 | 2.03 | 0.0011 | 137 |
| Pt | Pt | 3.7 | 2.75 | 0.0023 | |
| Pt | Rh | 0.7 | 2.70 | 0.0004 | |
| Pt | O | 0.7 | 2.00 | 0.0008 | 183 |
| Pt | Pt | 4.1 | 2.73 | 0.0017 | |
| Pt | Rh | 1.1 | 2.70 | 0.0039 | |
| Pt | O | 0.5 | 2.03 | 0.0010 | 213 |
| Pt | Pt | 4.3 | 2.72 | 0.0016 | |
| Pt | Rh | 1.2 | 2.71 | 0.0028 | |
| Pt | Pt | 4.4 | 2.73 | 0.0027 | 300 |
| Pt | Rh | 1.4 | 2.72 | 0.0034 | |
| Pt | Pt | 5.1 | 2.74 | 0.0033 | 300/1 h |
| Pt | Rh | 1.9 | 2.71 | 0.0014 | |

The contribution at 1.95 Å disappeared from RT to 90 °C, while a new contribution was not observed. At 95 °C, two metal−metal signals, **Pt**−Pt and **Pt**−Rh, appeared simultaneously. The average Pt environment was made up of 3.1 O at 2.02 Å, 0.4 Rh at 2.68 Å, and 2.1 Pt at 2.70 Å. The **Pt**−Rh + Pt−Pt coordination number suggests (after correction for the presence of Pt−O) that very small metal clusters are formed. Figure 8 compares the fits obtained with and without making use of the metal−metal contributions. Apparently, some small bimetallic particles had been formed. The contraction of the interatomic distances (Table 2) relative to bulk metals is attributed to the reduced size of the clusters, as reported before.[28] From 100 to 200 °C a constant increase in the metal−metal coordination numbers and a decrease in the Pt−O contribution took place. Even after the O signal had disappeared (∼220 °C), the metal−metal contributions still increased, and a small increase continued even during the isothermal reduction at 300 °C. At the end, the CNs were 5.1 and 1.9 and the interatomic distances 2.74 and 2.71 Å for the **Pt**−Pt and **Pt**−Rh contributions, respectively.

Qualitative and quantitative analyses were also performed on sample B, the monometallic Pt sample. The FT profiles are presented in Figure 9, and the quantitative results in Table 3 and Figure 10. In this case, a slow formation and gradual growth of Pt monometallic clusters took place from 83 to 300 °C. The FT profiles of samples A and B (at the Pt edge) were clearly different when the metal−metal shell began to appear, confirming that the **Pt**−Rh contribution in the bimetallic sample

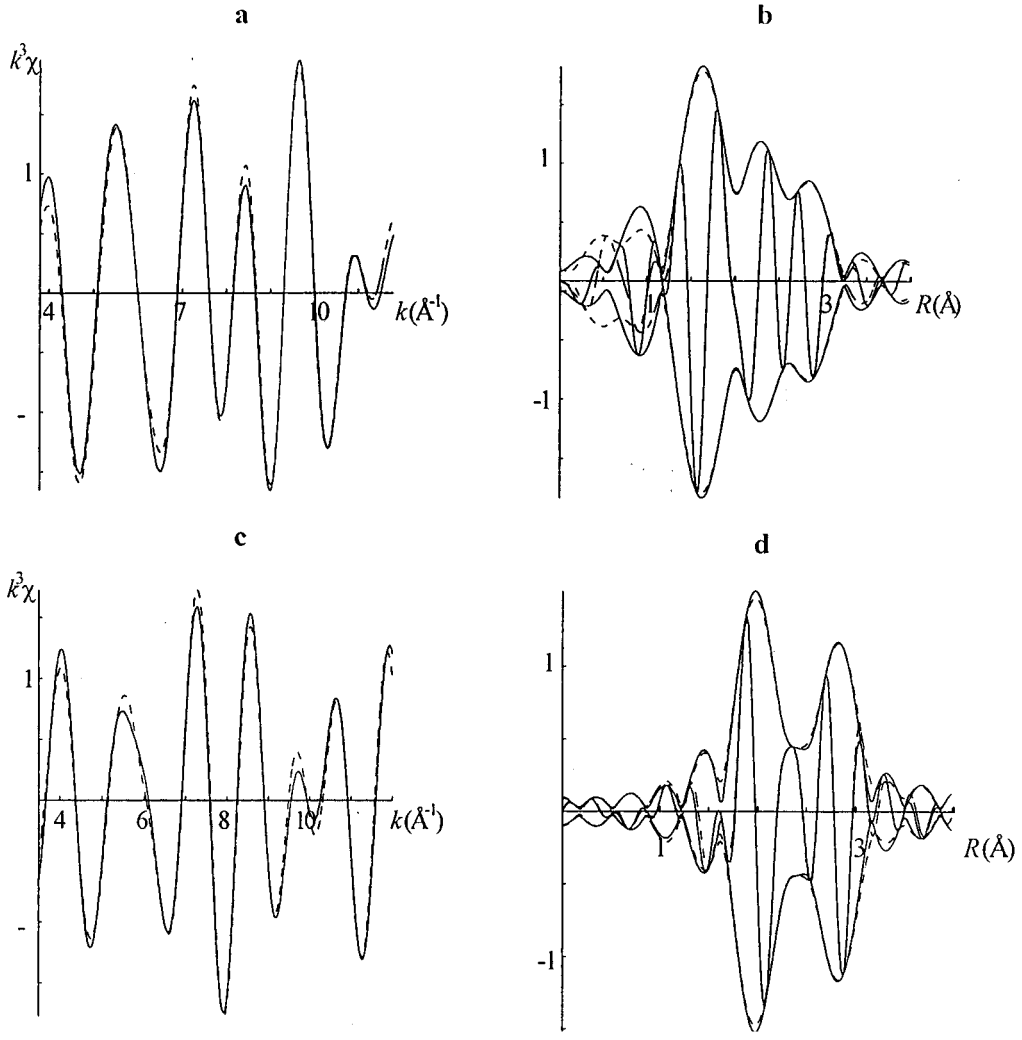


**Figure 7.** Sample A (Pt edge) during reduction: measured signals (—) and corresponding fits (− − −) of $\chi(k)k^3$ and related FT at 213 °C (**a** and **b**, respectively) and after 1 h at 300 °C (**c** and **d**, respectively).

is present *from the beginning* of the formation of the metal clusters. In sample B a Pt−Pt signal at 2.1 Å appears at 83 °C, attributed to the Pt particles as they are forming. The small Pt−O contribution at 2.74 Å, which is present at 300 °C, was assigned to the interaction between Pt atoms and $O^{2-}$ ions present in the framework of the zeolite, as observed in the accompanying normal EXAFS study [8] and as found in similar samples.[12,29]

## Discussion

Before discussing the results, an estimate of the reliability of the method and the uncertainty of the quantitative results must be given. A rigorous valuation should include many factors, some of which are not really quantifiable. Thus, as already mentioned, the sample changes during the 1 min recording of the spectrum, and the spectra could only be measured over a relatively small energy range. These factors should be taken into account when analyzing the results. On the other hand, some checks on the data reliability were performed. First, certain conditions[30] concerning the EXAFS analysis of bimetallic samples, that is $N_{\mathbf{Pt}-\mathrm{Rh}}X_{\mathrm{Pt}} = N_{\mathbf{Rh}-\mathrm{Pt}}X_{\mathrm{Rh}}$ (where $N_{\mathbf{Pt}-\mathrm{Rh}}$ and $N_{\mathbf{Rh}-\mathrm{Pt}}$ represent the coordination numbers of heteroatomic pairs, and $X_{\mathrm{Pt}}$ and $X_{\mathrm{Rh}}$ the atomic fractions of Rh and Pt in the sample) and $R_{\mathbf{Pt}-\mathrm{Rh}} = R_{\mathbf{Rh}-\mathrm{Pt}}$ (where $R_{\mathbf{Pt}-\mathrm{Rh}}$ and $R_{\mathbf{Rh}-\mathrm{Pt}}$ represent the interatomic Pt−Rh distances measured at the Pt and Rh edge, respectively) were verified. In addition, spectra of fully reduced samples were subsequently recorded at liquid nitrogen temperature, in a normal EXAFS setup (45 min/scan) and analyzed. The results were very similar to those obtained from the QEXAFS analysis at the end of the reduction. In general, an error of 20% in the coordination numbers and of 0.03 Å in the interatomic distances was estimated. Within this range of uncertainty, the two conditions mentioned above were always respected.

The reduction of the Rh atoms consists of two steps. First, three quarters of the atoms are quickly reduced at 40 °C, giving rise to small monometallic clusters. Second, from about 100 to 300 °C, at the end of the reduction, a gradual reduction of the remaining Rh atoms was accompanied by the formation of bimetallic clusters. At the Pt edge, however, there was no clear step. From about 90 °C to the final reduction temperature, gradual reduction leading to the formation and gradual growth of bimetallic particles was observed.

Considering the results obtained at both edges, we infer that a substantial part of the particles of $Rh_2O_3$ presumably contained in the supercages of the NaY zeolite are quickly reduced at 40 °C, probably autocatalytically (the first reduced atoms catalyzed the further reduction of the oxide particles). The quick reduction of a considerable amount of cations is proven by the TPR spectrum of sample A (Figure 11), which presents a sharp peak at 40 °C, overlapping at high temperature with a broader peak. The latter has its maximum at 150 °C and continues beyond 200 °C. The form of this TPR spectrum is very consistent with our EXAFS results. The sharp peak is assigned to the reduction

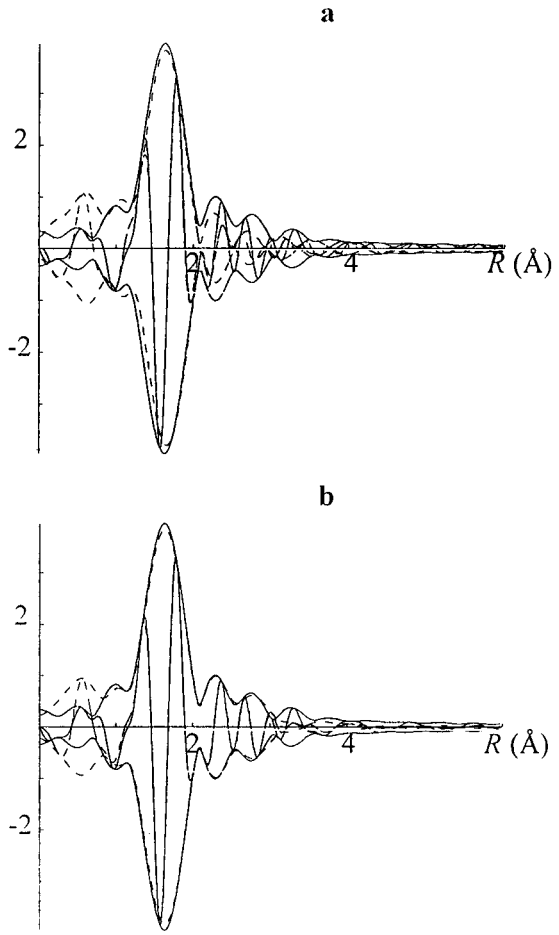


**Figure 8.** Sample A during reduction at 95 °C (Pt edge): FT of $\chi(k)k^3$ (—) and corresponding fits (− − −) without (**a**) the Pt−Pt and **Pt**−Rh contributions (variance of fit = 0.0136) and with (**b**) the Pt−Pt and **Pt**−Rh contributions (variance of fit = 0.0042).

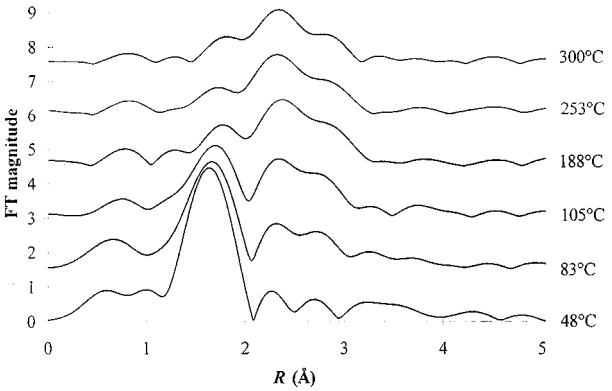


**Figure 9.** Evolution of the FT of $\chi(k)k^3$ measured at the Pt edge during reduction of sample B.

of Rh cations, as deduced from a comparison of the spectrum of sample A with the TPR spectra of the monometallic Rh and Pt samples (Figure 11).

Once formed, the metal clusters (20−25 atoms) could not escape from the supercages. Some Rh remained in the oxidic form, i.e., situated in other cages of the zeolite or mixed with Pt oxides. Up to 90 °C we did not detect the presence of Pt−Pt or **Pt**−Rh bonds, although the Pt−O signals decreased. Two reactions, not mutually exclusive, could account for that: on one hand the reduction of $Pt^{IV}$ to $Pt^{II}$ and on the other the reduction of $Pt^{2+}$ to isolated $Pt^0$ atoms.

The formation of small bimetallic particles at about 100 °C was proven by the **Pt**−Rh contributions detected at both edges.

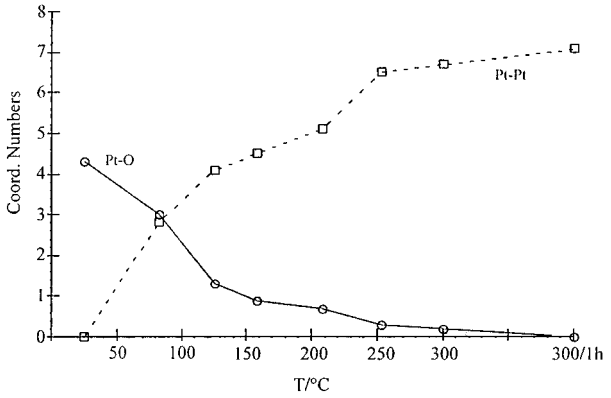


**Figure 10.** Evolution of the coordination numbers of sample B (Pt edge) during reduction.

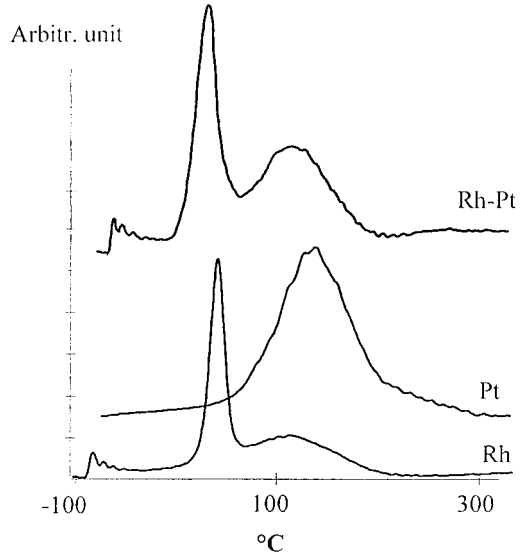


**Figure 11.** Temperature-programmed reduction (TPR) of the RhPt bimetallic sample A and the monometallic Rh and Pt samples.

**TABLE 3: Structural Parameters of Sample B at the Pt Edge during Reduction (Fits: $\Delta k = 3-11.7$ Å$^{-1}$, $\Delta R = 1-3$ Å, Variance ≈ 0.003)**

| absorb | backsc | *CN* | *R* (Å) | $\Delta\sigma^2$ | *T* (°C) |
|---|---|---|---|---|---|
| Pt | O | 1.1 | 1.97 | 0.0025 | RT |
| Pt | O | 3.2 | 2.02 | 0.0016 | |
| Pt | O | 3.0 | 2.01 | 0.0023 | 83 |
| Pt | Pt | 2.8 | 2.75 | 0.0047 | |
| Pt | Pt | 1.0 | 3.07 | 0.0018 | |
| Pt | O | 1.3 | 2.03 | 0.0014 | 126 |
| Pt | Pt | 4.1 | 2.76 | 0.0016 | |
| Pt | O | 0.9 | 2.07 | 0.0018 | 158 |
| Pt | Pt | 4.5 | 2.75 | 0.0014 | |
| Pt | O | 0.7 | 2.06 | 0.0017 | 208 |
| Pt | Pt | 5.1 | 2.74 | 0.0027 | |
| Pt | O | 0.3 | 2.04 | 0.0017 | 253 |
| Pt | Pt | 6.5 | 2.74 | 0.0031 | |
| Pt | O | 0.2 | 2.04 | 0.0008 | 300 |
| Pt | Pt | 6.7 | 2.74 | 0.0018 | |
| Pt | O | 0.4 | 2.75 | 0.0014 | |
| Pt | Pt | 7.1 | 2.74 | 0.0023 | 300/1 h |
| Pt | O | 0.5 | 2.75 | 0.0034 | |

The difference between the spectra of samples A and B further confirms the presence of Rh atoms in the coordination shell of the Pt atoms. While in sample B a Pt−Pt peak is observed, which grows during reduction, in sample A the Pt−Pt signal is accompanied from the beginning by a **Pt**−Rh signal. The disappearance of the Rh−O signal concurrent with the formation of the bimetallic particles (from ∼100 °C to the end of the reduction) suggests that the Rh atoms which are still in the oxidic

form are reduced slowly together with the Pt atoms, giving rise to the bimetallic clusters. These small clusters are Pt-rich. The slow increase in the coordination numbers at the Pt edge suggests a gradual reduction of the oxidic particles and their successive merging. The absence of a step seems to indicate a similar behavior for all (different) oxidic Pt species with respect to cluster formation. It is noteworthy that the growth of the particles continues after the Pt−O contribution has disappeared, indicating that the growth of the bimetallic clusters continues by diffusion of metal particles through the channels of the zeolite. At the Rh edge, the presence of the large Rh−Rh contribution makes the spectra less sensitive to the small variations caused by the enlargement of the bimetallic particles (i.e., the **Rh**−Pt signal is detected 10 °C later). The bimetallic clusters which move through the channels probably meet also the large Rh monometallic clusters situated in the supercages, covering part of them with a bimetallic Pt-rich layer.

The diffusion (and subsequent merging) of particles through the channels must stop when the particle size exceeds the size of the entrances of the supercages (7.4 Å). From that point on, only a further merging with particles that can still enter the supercage is possible. At the end one expects to have clusters which just fit the supercages.[8,31,32] Different cluster structures are, however, possible. Some may have a Rh core, or may even be completely monometallic Rh particles formed at the beginning of the reduction (40 °C); others may be Pt-rich bimetallic particles, forming and growing slowly throughout the reduction process.

The Debye−Waller factors (Tables 1 and 2) show an inconsistent trend, which may be caused by two factors. First, they actually represent the difference between the sample and the reference compound; in our case we used different reference spectra which only in a first approximation were measured at the same temperature as the sample. Second, our sample is dynamic, with clusters that meet, merge, and sinter; therefore, the average "disorder" of the metal bond is not constant.

## Conclusions

The QEXAFS technique proved to be a very powerful tool for investigating the formation and growth of metal particles supported on a zeolite. In particular, it allowed us to follow the fate of the Rh and Pt atoms in a semiquantitative way, and, by explaining the different steps of cluster formation, it enabled us to understand their final structure.

Because EXAFS data are average results and can usually be fitted with more than one model, great care must be taken when formulating a model based on EXAFS data only. In the case of a nonhomogeneous distribution of the metal atoms, the composition of the particles can easily be misunderstood by looking at the normal EXAFS data only. In our system, the QEXAFS analysis proved the existence of monometallic Rh as well as bimetallic RhPt clusters, thus complementing and perfecting the conclusions reached in the standard EXAFS studies.

## References and Notes

(1) Meitzner, G.; Via, G. H.; Lytle, F. W.; Sinfelt, J. H. *J. Chem. Phys.* **1983**, *78*, 2533.
(2) Short, D. R.; Mansour, A.; Cook, J. W.; Sayers, D. E.; Katzer, J. R. *J. Catal.* **1983**, *82*, 299.
(3) Kip, B. J.; Duivenvoorden, F. B. M.; Koningsberger, D. C.; Prins, R. *J. Am. Chem. Soc.* **1986**, *108*, 5633.
(4) Ichikawa, M.; Fukushima, T.; Yokoyama, T.; Kosugi, N.; Kuroda, H. *J. Phys. Chem.* **1986**, *90*, 1222.
(5) Kampers, F. W. H.; Engelen, C. W. R.; van Hooff, J. H. C.; Koningsberger, D. C. *J. Phys. Chem.* **1990**, *94*, 8574.
(6) Ahn, D. H.; Lee, J. S.; Nomura M.; Sachtler, W. M. H.; Moretti, G.; Woo, S. I.; Ryoo, R. *J. Catal.* **1992**, *133*, 191.
(7) Via, G. H.; Sinfelt, J. H. *X-ray Absorption Fine Structure for Catalysts and Surfaces;* Iwasawa, Y., Ed.; World Scientific: Singapore, 1996; p 147.
(8) Cimini, F.; Prins, R. *J. Phys. Chem. B* **1997**, *101*, 5285.
(9) Moonen, J.; Slot, J.; Lefferts, L.; Bazin, D.; Dexpert, H. *Physica B* **1995**, *209*, 689.
(10) Frahm R. *Rev. Sci. Instrum.* **1989**, *60*, 2515.
(11) Bazin, D; Dexpert, H.; Lagarde, P.; Bournonville, J. P. *J. Catal.* **1988**, *110*, 209.
(12) Tzou, M. S.; Teo, B. K.; Sachtler, W. H. *J. Catal.* **1988**, *113*, 220.
(13) Bazin, D.; Dexpert, H.; Guyot-Sionnest, N. S.; Bournonville, J. P.; Lynch, J. *J. Chim. Phys.* **1989**, *86*, 1707.
(14) Homeyer, S. T.; Sachtler, W. H. *J. Catal.* **1989**, *117*, 91.
(15) Kampers, F. W. H.; Maas, T. M. J.; van Grondelle, J.; Brinkgreve, P.; Koningsberger, D. C. *Rev. Sci. Instrum.* **1989**, *60*, 2635.
(16) Kampers, F. W. H.; Engelen, C. W. R.; van Hooff, J. H. C.; Koningsberger, D. C. *J. Phys. Chem.* **1990**, *94*, 8574.
(17) Vaarkamp, M.; Linders, J. C. ; Koningsberger, D. C. *Physica B* **1995**, *209*, 159.
(18) Mustre de Leon, J.; Rehr, J. J.; Zabinsky, S. I.; Albers, R. C. *Phys. Rev. B* **1991**, *44*, 4146.
(19) Stern, E. A.; Bunker, B. A.; Heald, S. H. *Phys. Rev. B* **1980**, *21*, 5521.
(20) Meitzner, G.; Via, G. H.; Lytle, F. W.; Sinfelt, J. H. *J. Chem. Phys.* **1985**, *83*, 353.
(21) Asakura, K.; Yamazaki, Y.; Kuroda, H.; Harada, M.; Toshima, N. *Jpn. J. Appl. Phys.* **1993**, *32*, 448.
(22) Sayers, D. E.; Stern, E. A. *Phys. Rev. B* **1983**, *27*, 1017.
(23) Crozier, E. D.; Rehr, J. J.; Ingalls, R. *X-ray Absorption*; Koningsberger, D. C., Prins, R., Eds.; John Wiley and Sons: New York, 1988; pp 395−403.
(24) Tomczac, D. C.; Lei, G. D.; Schünemann, V.; Treviño, H.; Sachtler, W. M. H. *Microporous Mater.* **1996**, *5*, 2632.
(25) Tomczak, D. C.; Zholobenko, V. L.; Lei, G.-D.; Sachtler, W. M. H. *Stud. Surf. Sci. Catal.* **1994**, *84*, 893.
(26) Siegel, S.; Hoekstra, H. R.; Tani, B. S. *J. Inorg. Nucl. Chem.* **1968**, *31*, 3803.
(27) Park, S. H.; Tzou, M. S.; Sachtler, W. M. H. *Appl. Catal.* **1986**, *24*, 85.
(28) Apai, G.; Hamilton, J. F.; Stohr, J.; Thompson, A. *Phys. Rev. Lett.* **1979**, *43*, 165.
(29) Moller, K.; Koningsberger, D. C.; Bein, T. *J. Phys. Chem.* **1989**, *93*, 6116.
(30) Via, G. H.; Drake Jr., K. F.; Meitzner, G.; Lytle, F. W.; Sinfelt, J. H. *Catal. Lett.* **1990**, *5*, 25.
(31) Kleine, A.; Ryder, P. *Catal. Today* **1987**, *3*, 103.
(32) Cimini, F.; Prins, R. *Physica B* **1995**, *209*, 699.